World Electric Vehicle Journal

MDPI

Article

Optimal Load Sharing between Lithium-Ion Battery and Supercapacitor for Electric Vehicle Applications

Hegazy Rezk [1,*] and Rania M. Ghoniem [2]

[1] Department of Electrical Engineering, College of Engineering in Wadi Alddawasir, Prince Sattam bin Abdulaziz University, Al-Kharj 11942 , Saudi Arabia
[2] Department of Information Technology, College of Computer and Information Sciences, Princess Nourah bint Abdulrahman University, P.O. Box 84428, Riyadh 11671, Saudi Arabia; rmghoniem@pnu.edu.sa
* Correspondence: hr.hussien@psau.edu.sa

Abstract: There has been a suggestion for the best energy management method for an electric vehicle with a hybrid power system. The objective is to supply the electric vehicle with high-quality electricity. The hybrid power system comprises a supercapacitor (SC) bank and a lithium-ion battery. The recommended energy management plan attempts to maintain the bus voltage while providing the load demand with high-quality power under various circumstances. The management controller is built on a metaheuristic optimization technique that enhances the flatness theory-based controller's trajectory generation parameters. The SC units control the DC bus while the battery balances the power on the common line. This study demonstrates the expected contribution using particle swarm optimization and performance are assessed under various optimization parameters, including population size and maximum iterations. Their effects on controller performance are examined in the study. The outcomes demonstrate that the number of iterations significantly influences the algorithm's ability to determine the best controller parameters. The results imply that combining metaheuristic optimization techniques with flatness theory can enhance power quality. The suggested management algorithm ensures power is shared efficiently, protecting power sources and providing good power quality.

Keywords: electric vehicle; optimization; Li-ion battery; supercapacitor

check for updates

Citation: Rezk, H.; Ghoniem, R.M. Optimal Load Sharing between Lithium-Ion Battery and Supercapacitor for Electric Vehicle Applications. *World Electr. Veh. J.* **2023**, *14*, 201. https://doi.org/10.3390/wevj14080201

Academic Editors: Rongheng Li and Xuan Zhou

Received: 19 June 2023
Revised: 22 July 2023
Accepted: 25 July 2023
Published: 27 July 2023

1. Introduction

Increased urban development leads to increased emissions from transportation, which can complicate efforts to maintain a stable scenario of limiting global temperature increases to 1.5 °C [1]. As a result, the transportation sector will undergo adjustments due to society's efforts to reduce its carbon footprint as a response to climate change by the year 2050 [2]. The transportation industry is gradually converting from traditional fossil fuels to low-emission substitutes based on electric vehicle (EV)-based batteries or hydrogen fuel cell technology as the energy supply system [3]. The market for EVs is now seeing significant growth. EVs are becoming increasingly popular due to advancements in battery technology and increased range [4]. In addition, the price of the battery, the most expensive part of the electric vehicle propulsion system, has decreased by about 90% [5]. Moreover, the driving distance grew from 100 to 150 km to 400 km or more [6,7]. These impressive improvements make EVs an excellent choice for transport decarbonization.

Hybridization between batteries and supercapacitors, known as a hybrid power system (HPS), is necessary to meet all EVs' requirements and deliver optimum performance. This hybridization offers numerous advantages, including energy density, power density, discharge rate, life cycle, and cost [8]. Generally, the battery can store a lot of energy. However, it cannot provide much power quickly because of its poor power output density, while the SC has a small storage capacity but can provide a big burst of power [9]. The battery is utilized to provide a high-power supply at low loads, enhancing total efficiency, while the SC bank is employed to meet acceleration and regenerative braking demands. The SC and the battery can work together to provide the storage and peak current requirements. This is accomplished by combining these energy sources in parallel [10]. Due to peak utilization, batteries lose performance with time; hence, when EVs require unexpected energy demand when accelerating, the battery pack alone cannot provide this requirement. Moreover, significant currents are produced during regenerative braking, which might reduce battery lifetime [9]. Allocating these transit currents to the SC can improve the battery's lifetime. However, employing the HPS requires knowing the suitable topology and establishing an appropriate energy management strategy (EMS). In the case of active topology, the EMS generates two power references: The supercapacitor power reference, whose primary role is to stabilize the dc bus voltage, and the battery power reference generated according to the SC's SoC and the load power.

Based on the energy demand and the set-up of the DC-DC converters, HPS can be configured in passive, semi-active, or active topologies. In the passive topology, no power control circuits are involved; instead, the energy storage systems (ESS) are connected to the load in parallel. In the semi-active topology, just one DC-DC converter is used. Two DC-DC converters are employed in the active topology [11]. Concerning the EMS, there are two types [12]: online strategies such as rule-based, fuzzy logic, predictive models, and filtration-based are straightforward to apply in a real-world application. Offline strategies such as Pontryagin's minimal principle (PMP) and dynamic programming (DP) can provide globally optimal results. However, their usage in practical applications is complex due to their high computational costs [13].

Using flatness control theory to improve power quality has been successfully studied and improved [14,15]. Its basic approach is establishing a reduced-order model and designing a trajectory control law for the inverse dynamics of the reduced-order model. However, determining the parameters of the trajectory generation is a challenging task, and the classical methods can provide limited performance. In this study, optimizing the trajectory generation parameters using metaheuristic optimization algorithms (MOAs) will be assessed. Particle swarm optimization (PSO) is used since it is considered one of the most knowledgeable and widely used metaheuristic optimization algorithms. The performance of each algorithm will be investigated under different sizes and a variable number of iterations. As mentioned above, to extend the HPS lifecycle, the power quality on the common bus must be improved. In this paper, an optimized version of the flatness-based control strategy is proposed. The main contribution of this paper is the introduction of metaheuristic optimization algorithms to enhance the performance of a flat controller using the PSO, which improves the power quality of the HPS. This will reduce harmonics and extend the battery system's lifetime.

The rest of the paper is organized as follows: Section 2 presents a description of the HPS, including the topology and the system models. Section 3 explains the proposed EMS, the conventional flatness-based EMS presented, and the optimization manner of its control parameters. Section 4 presents the simulation results and the related discussion. This paper ends with a conclusion.

2. Configuration of the Power System

2.1. HPS Description

The HPS-based EV is made in an active topology to meet the engine power. The HPS comprises a lithium-ion battery and supercapacitor, as shown in Figure 1. The battery and the SC are connected to the DC bus through bidirectional DC/DC boost converters. On the other hand, the vehicle motor is powered by a bidirectional DC/AC converter, which allows power to flow in both directions, from the DC bus to the engine in the traction case and the reverse in the breaking scenario.

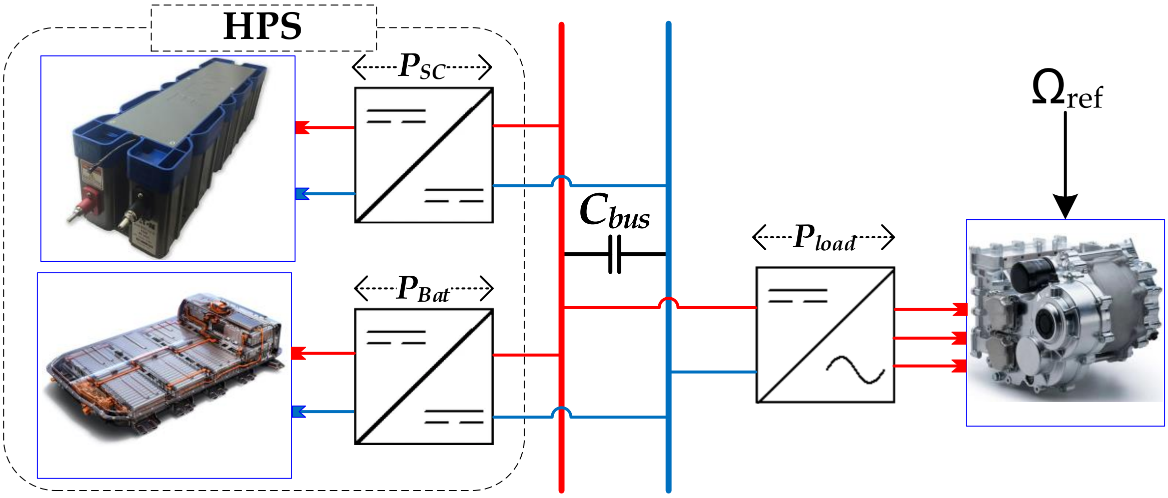

Figure 1. The HPS Power System Topology.

2.2. Vehicle Traction Model

The total traction forces (F_T) can be calculated as a function of the physical forces applied to the vehicle body [16]. It can be provided as

$$F_T = F_m + F_r + F_{ad} + F_U \tag{1}$$

where F_m is the motor force, F_r is the rolling resistance force, F_{aero} is the aerodynamic force, and F_U is the gradeability or uphill driving force. The formula of each force and the definition of its parameters is provided in Table 1.

Table 1. Forces and their parameters.

Force	Equation	Parameters
Motor force	$F_m = M_{equi}a = \left(m_v + J_{em}\frac{\rho^2}{R_{tire}^2}\right)\frac{dv(t)}{dt}$	a: the acceleration m_v: the vehicle mass J_{em}: the motor inertia ρ: the air density R_{tire}: the tire radius v: the vehicle speed
Rollin resistance force	$F_r = c_r m_v g \cos(\alpha)$	c_r: the rolling friction coefficient m_v: the vehicle mass g: the gravity acceleration α: the road slop
Aerodynamic force	$F_{aero} = \frac{1}{2}\rho v^2 A C_d$	ρ: the air density v: the vehicle speed A: the frontal area C_d: the drag coefficient
uphill driving force	$F_U = m_v g \sin(\alpha)$	m_v: the vehicle mass g: the gravity acceleration α: the road slop

The load power required by the traction engine on the DC bus can be expressed as a function of the electrical (η_{mot}), the mechanical transmission (η_{trans}), and the inverter efficiencies (η_{inv}) [17]. It can be formulated as

$$P_{load}(t) = P_T(t) \cdot \eta = v(t) \cdot F_T(t)\eta_{mot} \cdot \eta_{inv} \cdot \eta_{trans} \tag{2}$$

2.3. Li-Ion Battery Description and Modeling

Several electrochemical models exist in the literature, such as the Internal resistance battery model, the single RC network battery model (Thevenin model), and the Randles circuit [18]. The Shepherd model is one of the most commonly used models to express the electrical aspect [19]. The battery discharging voltage can be expressed as a function of the open circuit voltage (E_{oc}), the polarization voltage losses (V_{pol}), the exponential voltage losses (V_{exp}), and the ohmic losses (V_{ohm}). The output voltage and the state of charge (SoC) can be presented as

$$\begin{aligned} V_{dis} &= E_{OC} - \overbrace{K\frac{Q}{Q-it}(it+i^{*})}^{V_{pol}} + \overbrace{A.\mathrm{e}^{(-B*\mathrm{it})}}^{V_{exp}} - \overbrace{R_{\mathrm{int}}.i_{Bat}}^{V_{ohm}} \\ SoC(\mathrm{t}) &= SoC_0 - \frac{1}{Q}\int i_{Bat}dt \end{aligned} \tag{3}$$

where the battery parameters can be listed as follows

- K is a polarization constant,
- Q is the nominal capacity (Ah),
- it is the current battery charge (Ah),
- A denotes the exponential zone amplitude (V)
- B denotes the exponential zone time constant inverse in the exponential zone (Ah^{-1})
- R_{int} is the internal resistance (Ω),
- i and i^* are the battery current and the filtered current (A),
- SoC_0 is the initial state of charge.

The scheme of this model is illustrated in Figure 2.

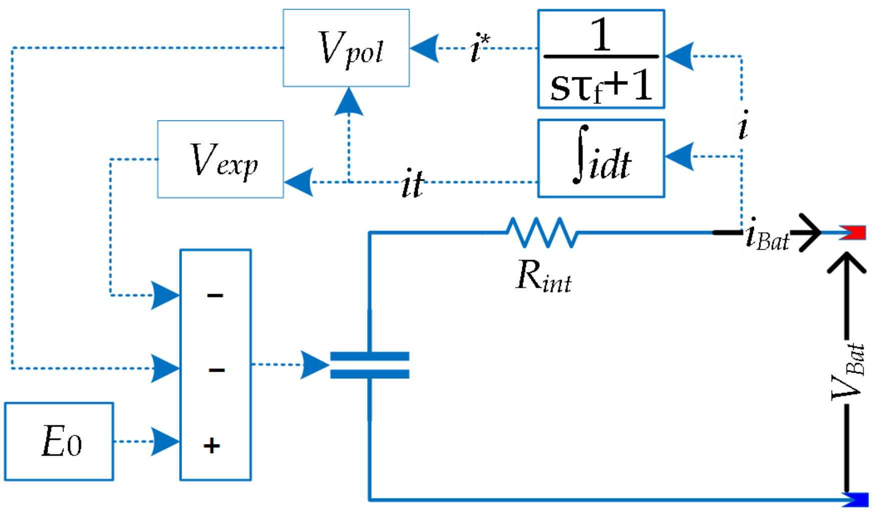

Figure 2. Li-ion Shepherd model.

2.4. Supercapacitor Description and Modeling

The supercapacitor (SC), also defined as the Ultracapacitor (UC) or double-layer capacitor, differs from the regular capacitor because it has substantial capacitance [20]. The supercapacitor stabilizes the DC bus energy as a fast, dynamic storage device. Thus, it is not a replacement for batteries to store long-term energy. Immediate supply for peak power is met by the SC. The SC provides the difference between load demand and battery power during short periods. According to ref. [20], the model of the SC consists of an equivalent series resistance R_S representing charging/discharging resistance, a capacitance C_{cell} representing the SC capacity, and an equivalent parallel resistance R_R representing self-discharge losses. Its output voltage and SoC are presented as reported in [21] as

$$\begin{aligned} V_{Cell} &= i_{Cell} R_S + \tfrac{1}{C_{sc}} \int i_c dt \\ SoC_{SC}(t) &= \left(\tfrac{V_{Cell}(t)}{V_{nom}} \right)^2 \end{aligned} \tag{4}$$

where V_{Cell} is the SC nominal voltage, the equivalent circuit of the SC unit is shown in Figure 3.

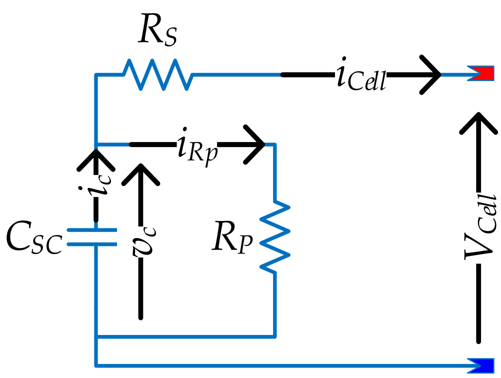

Figure 3. SC equivalent circuit model.

2.5. Power System Modeling

The dc bus energy (E_{bus}) must be adjusted to meet the desired value, where the dc energy is determined as a function of its voltage (v_{bus}) and capacitance (C_{bus}). Its equation can be formulated as:

$$E_{bus} = 0.5 \cdot C_{bus} v_{bus}^2 \tag{5}$$

On the other hand, the bus power can be presented as a function of the battery and the SC power as follows:

$$\dot{E}_{bus} = P_{Bat.\_out} + P_{SC\_out} - P_{load} \tag{6}$$

where P_{Bat_out} is the battery converter output power, P_{SC_out} is the SC converter output power, and P_{load} is the motor load power. They can be expressed as:

$$P_{Bat.\_out} = P_{Bat.} - r_{Bat} \left({P_{Bat.}}/{v_{Bat.}} \right)^2 \tag{7}$$

$$P_{SC.\_out} = P_{SC} - r_{SC} \left({P_{SC}}/{v_{SC}} \right)^2 \tag{8}$$

where r_{Bat} and r_{SC} are the battery's internal resistance and the SC converters.

3. The Proposed Energy Management System

3.1. Flatness Control Theory

Due to the system's nonlinearity, the linear control techniques may be more complicated. As a result, differential flatness theory was used to lower the order of the model. Consequently, the alternative model allows for the definition of the dynamics of the trajectories [15]. The reduced-order model may be written using flatness control theory as

$$\begin{aligned} x &= \varphi(y, \dot{y}, \ddot{y}, \cdots y^{\beta}) \\ y &= \chi(x, u, \dot{u}, \cdots u^{\alpha}) \\ u &= \psi(y, \dot{y}, \ddot{y}, \cdots y^{\beta+1}) \end{aligned} \quad (9)$$

where x, y, u are the state variables, the outputs and the inputs of the reduced flat model, φ, χ, Ψ are three mapping functions, respectively, α and β and are a limited number of derivations.

3.2. Flatness Control on the HPS

The reduced-order model for the EV nonlinear model is based on the studies reported in ref. [22–24]. From Equation (6), the SC power reference can be expressed as

$$\begin{aligned} P_{SC}^{ref} &= \dot{E}_{bus} + P_{load} - P_{Bat\_out.} \\ &= \dot{E}_{bus} + v_{bus} \cdot i_{load} - P_{Bat\_out.} \end{aligned} \quad (10)$$

The parameters of the reduced-order model can be expressed as

$$\begin{aligned} x &= v_{bus} \\ y &= E_{bus} \\ u &= P_{SC}^{ref} \end{aligned} \quad (11)$$

From Equation (5), the state variable can be expressed as

$$x = \sqrt{2v_{bus} / C_{bus}} = \sqrt{2y / C_{bus}} = \varphi(y) \quad (12)$$

Whereas the flat input can be concluded from Equations (5)–(8) as

$$u = 2P_{SC}^{\lim} \left[1 - \sqrt{1 - \sqrt{\frac{\dot{y} + \left(\sqrt{2y / C_{bus}} \right) \cdot i_{load} - P_{Bat\_out}}{P_{SC}^{\lim}}}} \right] = \psi(y, \dot{y}) \quad (13)$$

$$P_{SC}^{\lim} = \frac{4v_{SC}}{r_{SC}}$$

In the steady state, Equation (6) equals zero; in this case, the battery supplies the total load power. This means that the value of the SC power reference depends on the bus energy. A second-order filter-based generation trajectory law is applied to ensure the control of this flat variable.

$$\frac{d\left(y_{ref} - y\right)}{dt} + k_1\left(y_{ref} - y\right) + k_2 \int \left(y_{ref} - y\right) dt = 0 \quad (14)$$

where k_1 and k_2 are control parameters that usually calculated as

$$\begin{aligned} k_1 &= 2 \cdot \xi \cdot \omega_n \\ k_2 &= {\omega_n}^2 \end{aligned} \quad (15)$$

where ξ is a damping factor, and ω_n is the natural frequency.

On the other hand, using a PI controller, the battery supplies the load and maintains the SC voltage at the reference value. The battery power reference can be provided as

$$\begin{aligned} P_{Bat}^{ref} &= P_{load} + P_{SC}^{req} \\ P_{SC}^{req} &= k_p\left(SoC_{sc}^{ref} - SoC_{SC}\right) + k_i\int\left(SoC_{sc}^{ref} - SoC_{SC}\right)dt \end{aligned} \quad (16)$$

where SoC_{SC}^{ref} is the SC's SoC reference value, k_p and k_i are the PI controller parameters.

3.3. Trajectory Generation Parameters Optimization

Determining the numerical values of the trajectory generation parameters is challenging due to the absence of an exact model that imitates the physical system. For this reason, enhancing these parameters using metaheuristic optimization algorithms will be performed. The key idea is to generate random candidate solutions in a limited search space. These candidate solutions will be sent to the HPS, and based on its behavior, the sum square error (SSE) between the reference and the measured DC bus voltage will be calculated. The optimizers update the candidate solutions depending on the obtained SSE, representing the fitness value. The objective function formulation is presented as

$$min(f(t)) = \sum_{t=1}^{N}\left(E_{bus}^{ref} - E_{bus}(t)\right)^2 \quad (17)$$

3.4. Particle Swarm Optimization

Particle swarm optimization (PSO) is one of the most well-known metaheuristic algorithms. PSO was created by Kennedy and Eberhart [25] by imitating the behavior of a swarm of birds and a fish. The PSO is widely used due to its ease of implementation and limited number of parameters. Despite the algorithm's simplicity, it produced excellent results when used to tackle diverse optimization issues across practically all branches of science and engineering. The enormous number of research publications that employ the PSO confirms this. PSO is created by simulating birds flying in multidimensional space. It uses several particles (called search agents or individuals) that fly in the search space to identify the optimal solution. Simultaneously, the particles in their pathways are all looking for the best solution. Each particle (ith) tries to update its position based on its position (x_i), velocity (v_i), and the distance between it and its best one (p^{best}) or the global best (g^{best}). The following equation can modify the velocity of each agent:

$$\begin{aligned} v_i(t+1) = w \cdot v_i(t) + c_1 \cdot r_1(p_i^{best}(t) - x_i(t)) \\ + c_2 \cdot r_2(g^{best}(t) - x_i(t)) \end{aligned} \quad (18)$$

where w represents the inrtia weight, c_1 and c_2 defined as acceleration coefficients, r_1 and r_2 are random numbers in (0,1). The following equation can be used to update the particle's position after updating its velocity:

$$x_i(t+1) = x_i(t) + v_i(t+1) \quad (19)$$

The main steps of the PSO are presented in detail in Figure 4.

The PSO has been chosen in this paper for several reasons, including its simplicity of implementation and the limited number of arguments. However, the most interesting thing is that it is the only one that can escape from the local optima compared with other metaheuristic optimization algorithms such as the salp swarm algorithm (SSA), the coot algorithm (COOT), and the marine predator algorithm (MPA). The global scheme of the proposed EMS is presented in Figure 5.

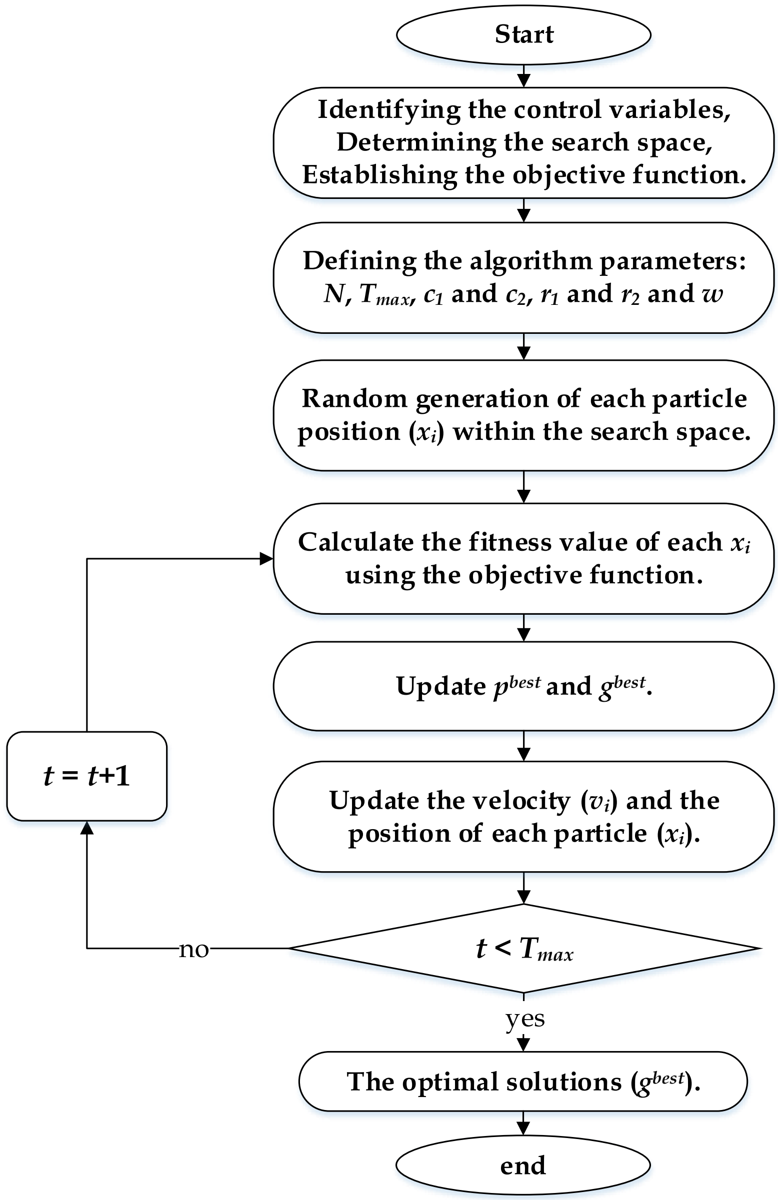

Figure 4. PSO general flow.

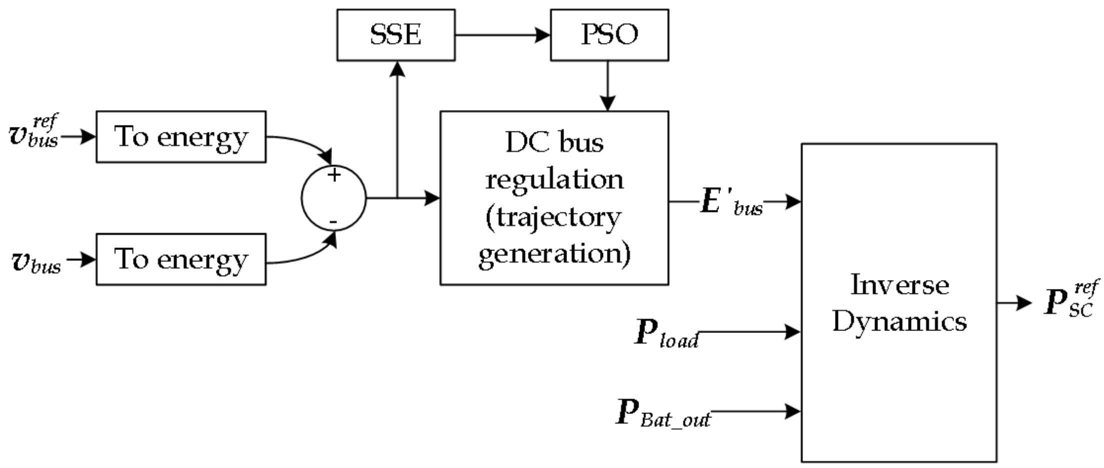

Figure 5. The structure of the proposed control law.

4. Results and Discussion

To approve the contribution of the proposed method, optimized versions of the flat controller will be applied to enhance the power quality of an HPS. The model of the proposed HPS is developed on Matlab, and its parameters are presented in Table 2 [26]. The considered engine load profile is shown in Figure 6. This profile includes both acceleration and breaking cases in a short time. The first 50 present a positive load demanded by the motor in the traction system. The power becomes negative (breaking case). This allows investigation of the system in both charging and discharging cases. The power becomes positive after t = 100 s.

Table 2. The hybrid power system (HPS) parameters.

Parameter	Value	Unit
DC bus voltage (v_{bus})	400	V
Battery nominal voltage	200	V
Battery rated capacity	1500	Ah
Battery internal resistance	1.3333	mΩ
SC rated voltage	200	V
SC rated capacity	120	F
DC-ERS	6.3	mΩ

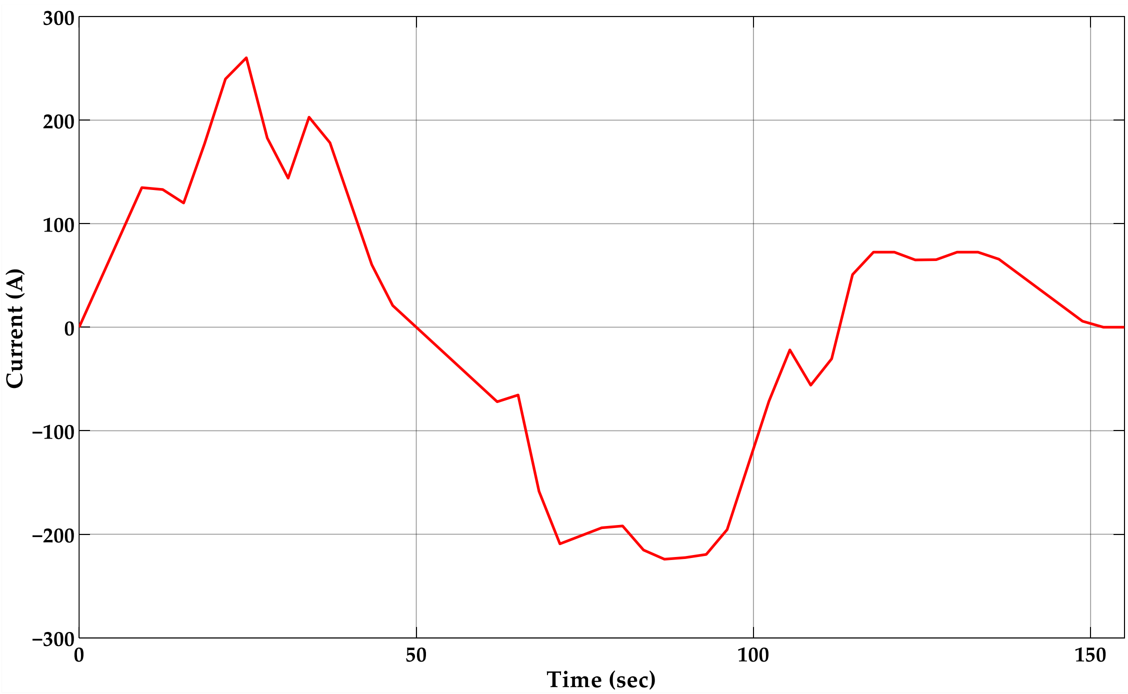

Figure 6. Motor load current (A).

The optimization problem has two optimization variables in a bi-dimensional search space. The evolution of the particles, as well as the global best (marked in bold and black) for various parameters, is presented below. The search space is a bi-dimensional search space where the upper limits are: $[50^2; 2 \times 0.6 \times 50] \times 10$, and the lower limits are $[50^2; 2 \times 0.6 \times 50] \times 0.1$. For T_{max} = 2, the evolution for N = 20, 25, and 30 is shown in Figure 7. Figure 8 illustrates their evolution for T_{max} = 30, whereas their evolution for T_{max} = 40 is presented in Figure 9.

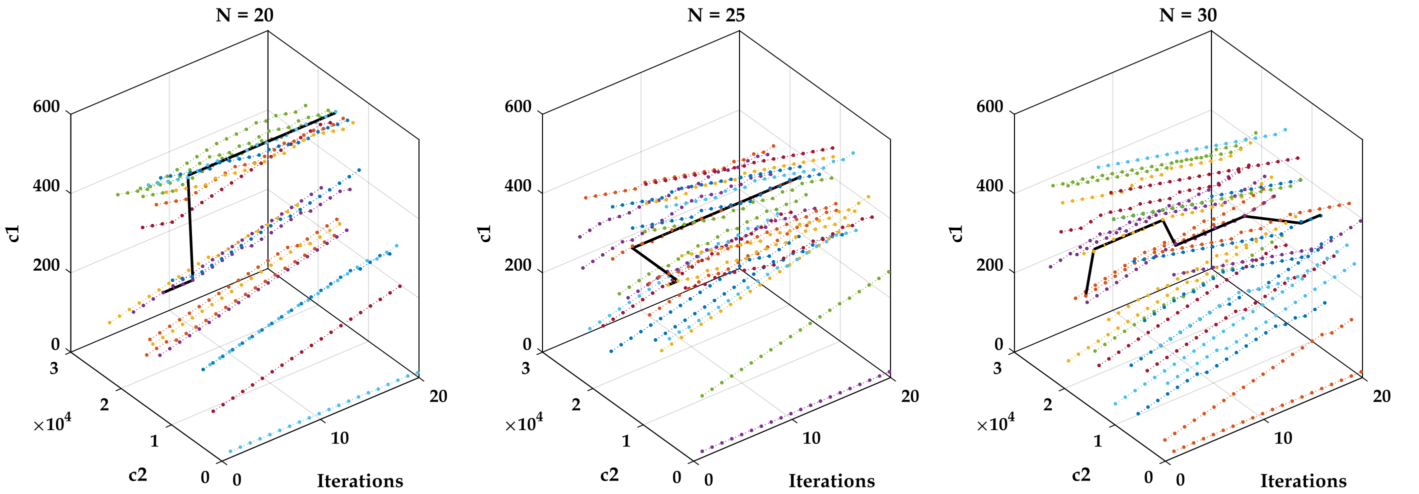

Figure 7. Particles and global best evolution for T_{max} = 20 and N = 20, 25 and 30.

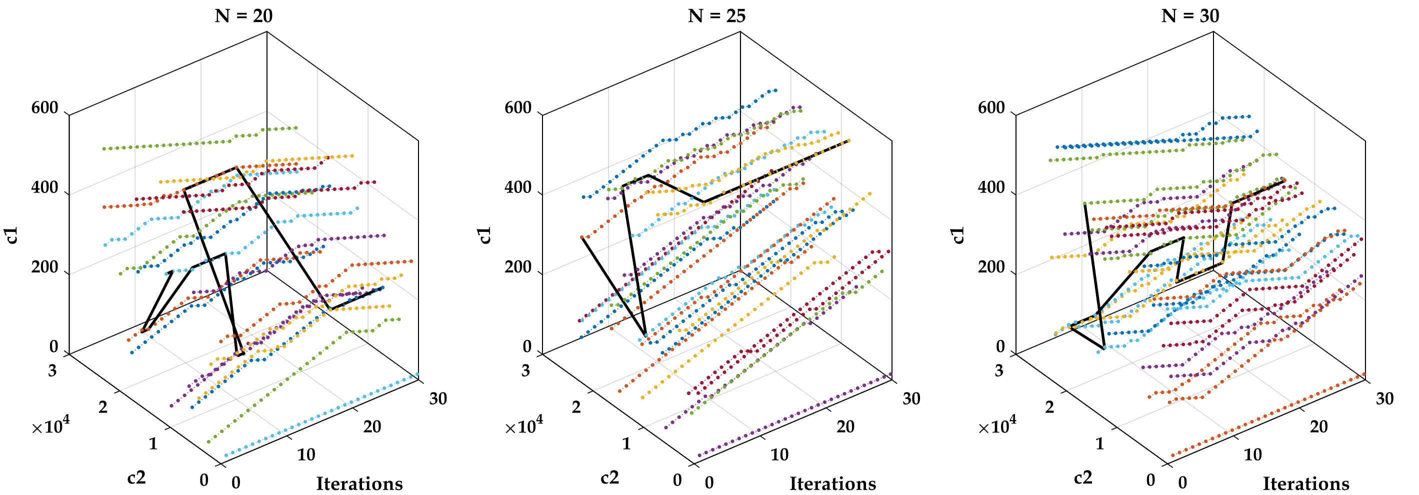

Figure 8. Particles and global best evolution for T_{max} = 30 and N = 20, 25 and 30.

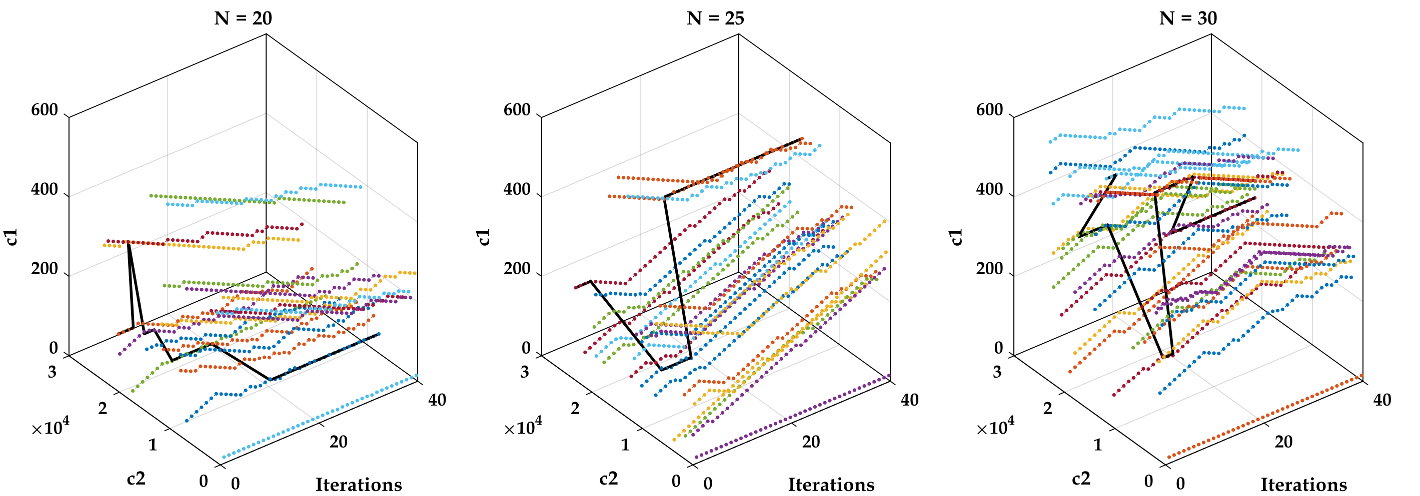

Figure 9. Particles and global best evolution for T_{max} = 40 and N = 20, 25 and 30.

From these figures, the global best shifts its position according to the received information from the other particles and the fitness of each one. It can be noticed that the rising maximum number of iterations of the population size affects the evolution of the global best position. From Figure 7, in cases $N = 20$ and $N = 25$, the global best falls into a local optimum, and the received information from the other particles is not enough to escape from it. However, a single run is insufficient to approve its results due to its stochastic behavior. Ten runs for each case have been performed, and the obtained results are presented and analyzed.

4.1. $N = 15$

Only 15 particles will be used in the population, with three numbers of iterations (20, 30, 40). The obtained results, including best, worst, mean, and standard deviation (STD), are presented in Table 3. The best results from these are marked in bold.

Table 3. The results for $N = 15$.

Parameter	T_{max} = 20			T_{max} = 30			T_{max} = 40		
Run	c_1	c_2	**Fitness**	c_1	c_2	**Fitness**	c_1	c_2	**Fitness**
1	383.0774	288.413	0.744101	15,222.15	141.1117	0.303494	24,189.45	165.2947	0.714826
2	2438.373	528.738	0.040471	848.3922	563.5098	0.372431	8865.301	83.49805	0.125425
3	7776.441	114.5011	0.233842	5429.146	194.2079	3.356814	8298.91	196.3338	0.041407
4	3703.151	368.4953	0.509587	1732.424	510.514	1.506235	7149.533	198.2457	0.060143
5	13,474.91	215.1098	0.193174	3937.523	448.4599	0.046181	3865.512	117.1225	0.276141
6	6445.147	514.2326	0.060138	6154.555	260.8997	0.041670	18,994.34	231.8808	0.040459
7	13,450.97	185.8164	1.261541	355.1203	365.4031	0.048072	14,981.46	146.3911	0.076724
8	4232.249	240.9958	0.041322	8334.283	104.0531	0.261079	5944.419	237.6877	0.042208
9	8190.019	111.7732	5.092025	20,151.94	235.7241	0.183018	19,443.92	221.3938	0.235585
10	9269.388	188.8361	0.0668	12,302.57	12.41503	0.5107	8661.424	391.4463	0.05599
Best			0.040471			0.041670			0.040459
Worst			5.092025			3.356814			0.714826
Mean			0.6630			0.8243			0.1669
STD			1.5507			1.0953			0.2102

Obviously, when the number of iterations rises, the accuracy of the obtained results increases, and the optimizer's robustness increases against its stochastic behavior, as confirmed by the STD results.

4.2. $N = 20$

In this case, 20 particles will be used in the population with three numbers of iterations (20, 30, 40). The obtained results are presented in Table 4. The best results from these are marked in bold.

Table 4. The results for $N = 20$.

Parameter	T_{max} = 20			T_{max} = 30			T_{max} = 40		
Run	c_1	c_2	**Fitness**	c_1	c_2	**Fitness**	c_1	c_2	**Fitness**
1	11,826.76	93.19765	2.245826	1361.706	450.704	0.87594	7739.252	283.6269	0.87594
2	14,837.47	156.4969	0.040997	15,500.24	203.0249	0.040704	7414.114	179.625	0.040704
3	5297.442	487.0256	1.951761	8875.964	172.0122	1.548547	23,109.18	282.9629	1.548547
4	4816.494	203.6002	0.055405	8700.802	337.4453	0.092213	13,219.59	218.262	0.092213
5	10,121.86	213.8215	0.126862	4794.793	291.548	0.042652	894.5254	454.2255	0.042652
6	5883.825	476.9306	0.12185	5459.857	200.4839	0.043839	24,525.24	240.4441	0.043839
7	7375.051	384.4963	0.442556	13,096.74	248.0717	0.075598	3564.287	150.9713	0.075598
8	4974.259	367.2208	0.09791	15,878.71	214.7461	0.040997	550.6795	472.2166	0.040444
9	5779.193	266.0327	2.425997	8730.815	319.7181	0.048494	18,777.06	214.7125	0.048494
10	9557.76	167.3051	0.051499	995.5619	409.6813	0.11786	866.7844	415.0205	0.11786
Best			0.040997			0.040704			0.040444
Worst			2.425997			1.548547			1.548547
Mean			0.756066			0.292684			0.292629
STD			1.0147			0.5106			0.2576

Similar to the previous case, when the number of iterations rises, the quality of the obtained results increases, and the STD value decreases.

4.3. N = 25

In this case, 25 particles will be used in the population. The obtained results are presented in Table 5. The best results from these are marked in bold.

Table 5. The results for N = 25.

Parameter	T_{max} = 20			T_{max} = 30			T_{max} = 40		
Run	c_1	c_2	Fitness	c_1	c_2	Fitness	c_1	c_2	Fitness
1	21,239.27	156.5408	0.199961	821.5885	302.5806	1.464763	3855.402	143.0495	0.070714
2	3252.432	432.9943	0.158742	4958.868	240.8672	0.054227	450.852	284.8996	0.124811
3	6478.996	149.5211	0.049922	6839.962	143.2368	0.520202	5347.225	343.5532	0.518617
4	5601.85	133.5292	0.73102	9794.622	154.9952	0.141705	4891.362	480.2033	0.060821
5	12,269.83	104.837	0.457274	8643.765	112.1261	0.850277	12,406.41	118.1735	0.260117
6	4562.328	73.11393	2.887429	6039.013	578.624	0.044073	22,572.78	139.345	0.426515
7	5026.632	286.4911	6.182282	9602.378	79.68568	0.65234	11,330.41	92.04818	0.042805
8	14,973.17	114.3648	6.56357	5243.316	370.1021	5.236458	4747.913	373.9807	0.062921
9	9656.716	149.2054	0.06042	21,962.56	172.9125	2.95518	4755.602	366.1609	0.070322
10	1033.751	514.0229	0.203469	7822.553	180.0342	0.167949	6877.921	177.4643	0.152653
Best			0.049922			0.044073			0.042805
Worst			6.56357			5.236458			0.518617
Mean			1.749409			1.208717			0.17903
STD			2.5796			1.6720			0.1681

Similar to the previous cases, when the number of iterations rises, the quality of the obtained results increases, and the STD value decreases. However, compared with the best result from the previous case (0.040444), the best result (0.042805) is not better due to the stochastic searching mechanism of the PSO.

4.4. N = 30

In this last case, the number of particles in the swarm is increased to 30. The obtained results are presented in Table 6. The best results from these are marked in bold.

Table 6. The results for N = 30.

Parameter	T_{max} = 20			T_{max} = 30			T_{max} = 40		
Run	c_1	c_2	Fitness	c_1	c_2	Fitness	c_1	c_2	Fitness
1	8354.616	212.3834	0.127434	3044.51	444.3849	0.346717	7067.059	237.6387	0.23582
2	7517.356	290.0919	0.326639	20,815.15	195.7481	0.110693	2859.644	356.6027	0.036413
3	4839.241	165.5752	0.203772	24,214.03	87.34257	0.050091	5593.393	508.3409	0.10063
4	8214.519	341.0167	0.217441	7519.267	179.8408	0.072317	12,603.48	164.4501	0.024219
5	5279.422	258.5353	0.155199	1079.613	469.6823	0.040409	440.3446	155.6074	0.041211
6	9634.918	228.373	0.126743	5276.985	115.2335	0.040706	1823.321	478.1531	0.043018
7	8398.724	229.1724	0.183014	10,393.05	109.113	1.320182	5527.736	429.3406	0.042232
8	10,275.87	276.8559	0.058362	2602.681	97.45093	0.046891	4213.783	510.2678	0.188963
9	14,010.6	149.9359	0.237414	2616.825	465.4587	0.564528	12,566.89	117.8922	0.775534
10	7711.38	503.7738	0.096414	23,525.33	153.5922	0.176081	9058.189	144.518	0.078604
Best			0.058362			0.040409			0.024219
Worst			0.326639			1.320182			0.775534
Mean			0.173243			0.276862			0.156664
STD			0.777			0.4044			0.2287

Similar to the previous cases, when the number of iterations rises, the quality of the obtained results increases, as does their robustness (STD decreased).

The results of the different combinations of the number of particles and the number of iterations are presented in Table 7 to easily see the best combination.

Table 7. The hybrid power system (HPS) parameters.

Population Size	Number of Iterations		
	20	**30**	**40**
15	0.040471	0.041670	0.040459
20	0.040997	0.040704	0.040444
25	0.049922	0.044073	0.042805
30	0.058362	0.040409	0.024219

From these results, the best combination is 40 iterations with a population size of 30 agents. This can be explained by the increased ability of exploitation (large population size) and exploration (large number of iterations).

The obtained results from another point will be compared in terms of population size. Figure 10 presents the fitness evolution for the same number of iterations (T_{max} = 20) and N = 15, 20, 25, and 30.

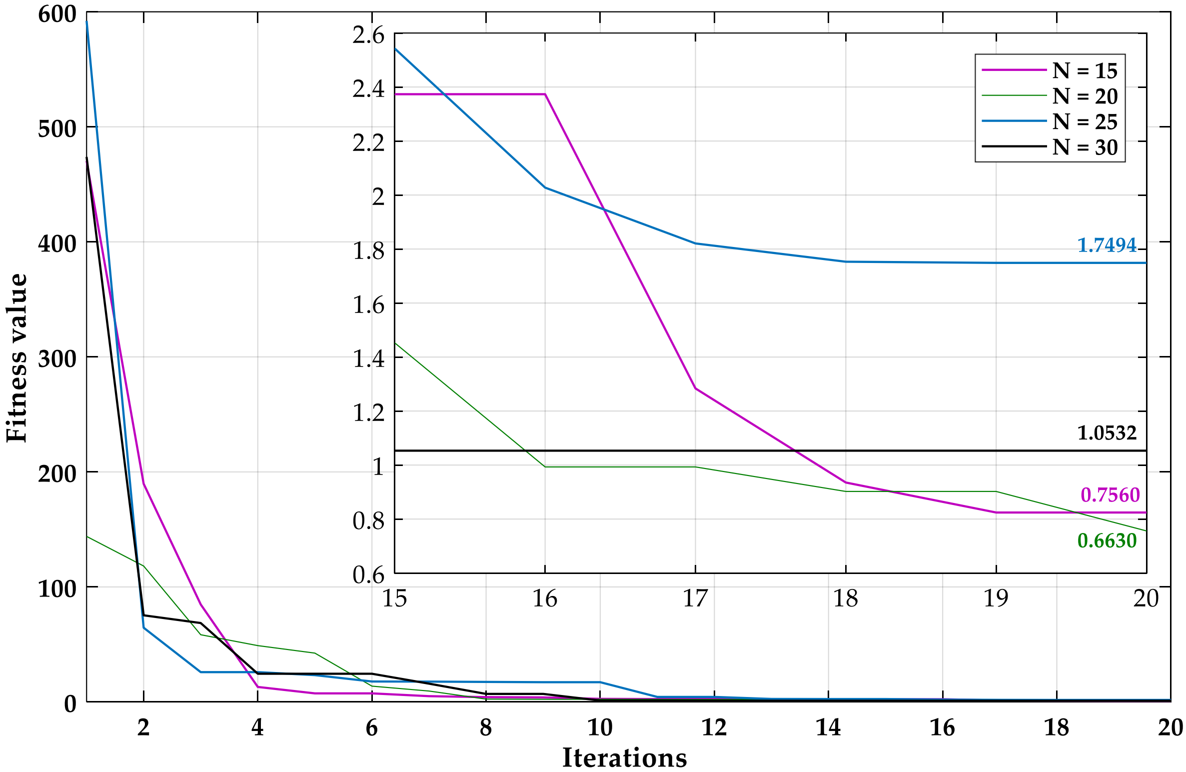

Figure 10. Fitness evolution for T_{max} = 20 iterations.

These curves show that the group with 20 particles provides the best results. This can be explained by the small number of iterations where random particle behavior affects their outcomes.

Figure 11 presents the fitness evolution for the same number of iterations T_{max} = 30.

These curves show that the group with 30 particles provides the best results. Rising the number of iterations increases the exploitation ability of the PSO, whereas expanding the population size increases its exploration ability. The results of the swarm that has 25 particles do not get the expected results because stochastic behavior affects its performance.

Finally, Figure 12 presents the fitness evolution for the same number of iterations T_{max} = 40. In this case, the swarm with 30 particles is expected to provide the best results due to the increased number of iterations.

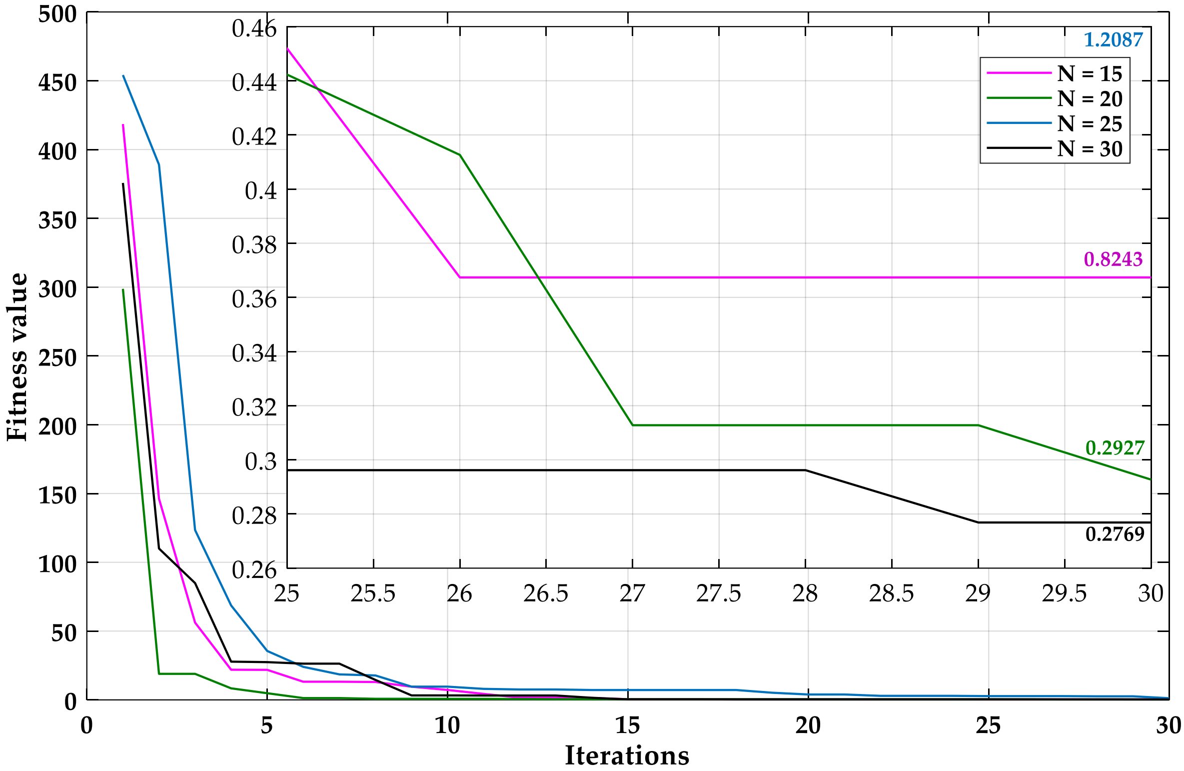

Figure 11. Fitness evolution for T_{max} = 30 iterations.

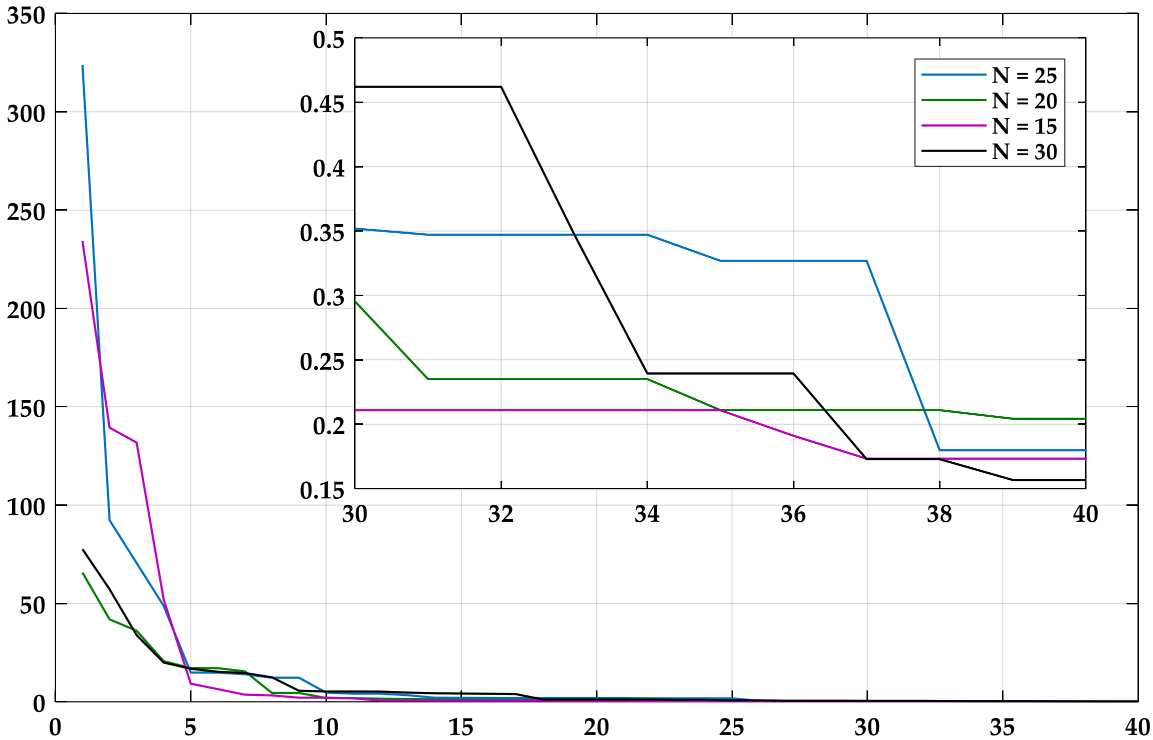

Figure 12. Fitness evolution for T_{max} = 40 iterations.

As the number of iterations increases, the personal best for each particle becomes closer to the global particle. After that, the results for the studied groups that included different population sizes became close. The curves in Figure 12 confirm the effect of the number of repetitions on PSO behavior compared with population size. Choosing the best combination of population size and max number of iterations is challenging in the metaheuristic optimization algorithm since there is no exact formula for determining them. They are chosen empirically. In addition, determining the search space limits in some applications is not easy.

The results of the best-optimized version of the flat controller are compared with those of the conventional one, where $c_1 = 50^2$ and $c_2 = 2 \times 0.6 \times 50$. The DC bus voltage for each controller is presented in Figure 13. From this figure, the fluctuations in the DC bus voltage have been successfully reduced using the optimized version compared with the conventional one.

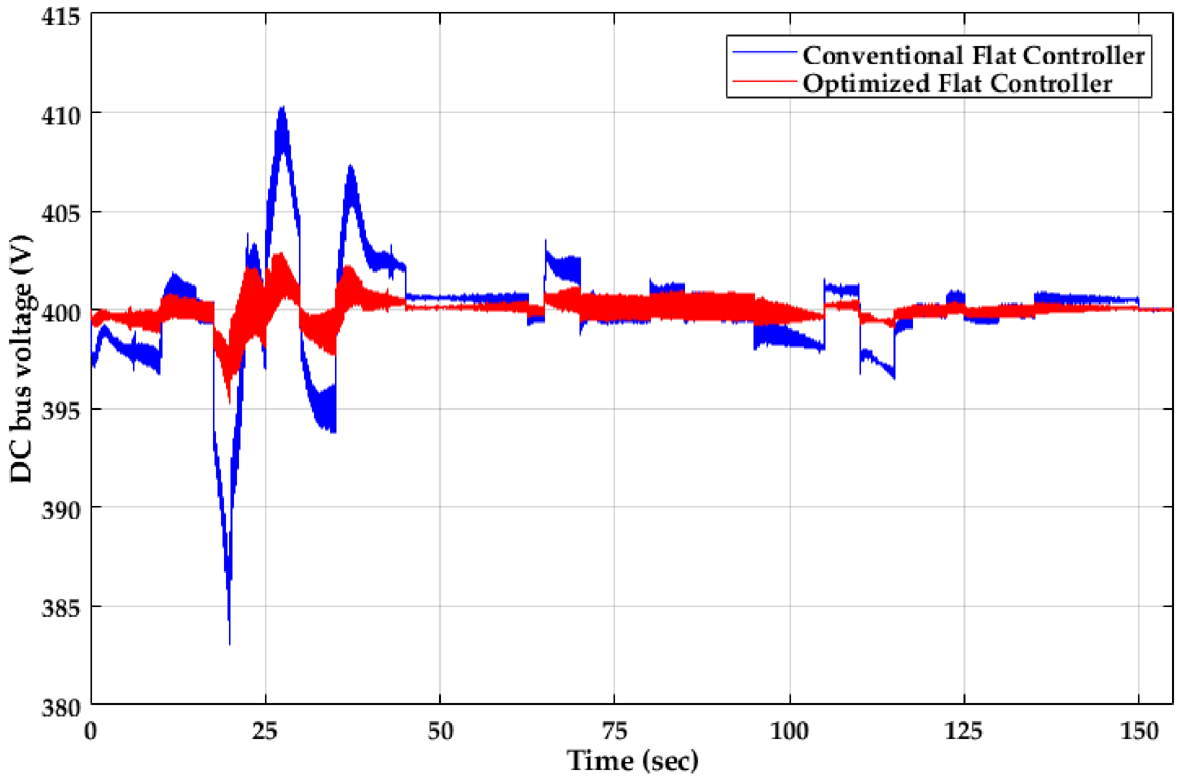

Figure 13. DC bus voltage using the conventional flat controller and the optimized version.

PSO successfully updates the parameters of the flat controller. The most exciting thing about this study is that the authors used other modern optimization algorithms such as the salp swarm algorithm (SSA), the coot algorithm (COOT), and the marine predator algorithm (MPA). Unlike the PSO, they did not contribute to developing suitable parameters for the flat console. This confirms the theory of no free lunch (NFL) [27]. In addition, using this optimized version of the control strategy for real-world applications can provide excellent performance for the HPS. However, its implementation requires fast calculators for using the PSO in online optimization mode. The rapid changes in load demand make it a very challenging task to optimize the control parameters in a short time. However, with technological advancement, the calculators' processing speed will significantly increase in the coming years. Moreover, the performance of the HPS can be further investigated, including more degrees of freedom, such as the power electronic converters, the battery degradation, and the motor constraints under more realistic profiles, as reported in [28].

The SC voltage is presented in Figure 14. The optimized controller successfully holds the DC voltage at the reference level, keeping its SoC at the desired value. Moreover, the battery SoC is illustrated in this figure. The battery discharges during the traction phase, where the SC voltage increases to maintain the DC voltage at the reference level. The battery SoC increases in the traction phase by absorbing the excess power in the common bus.

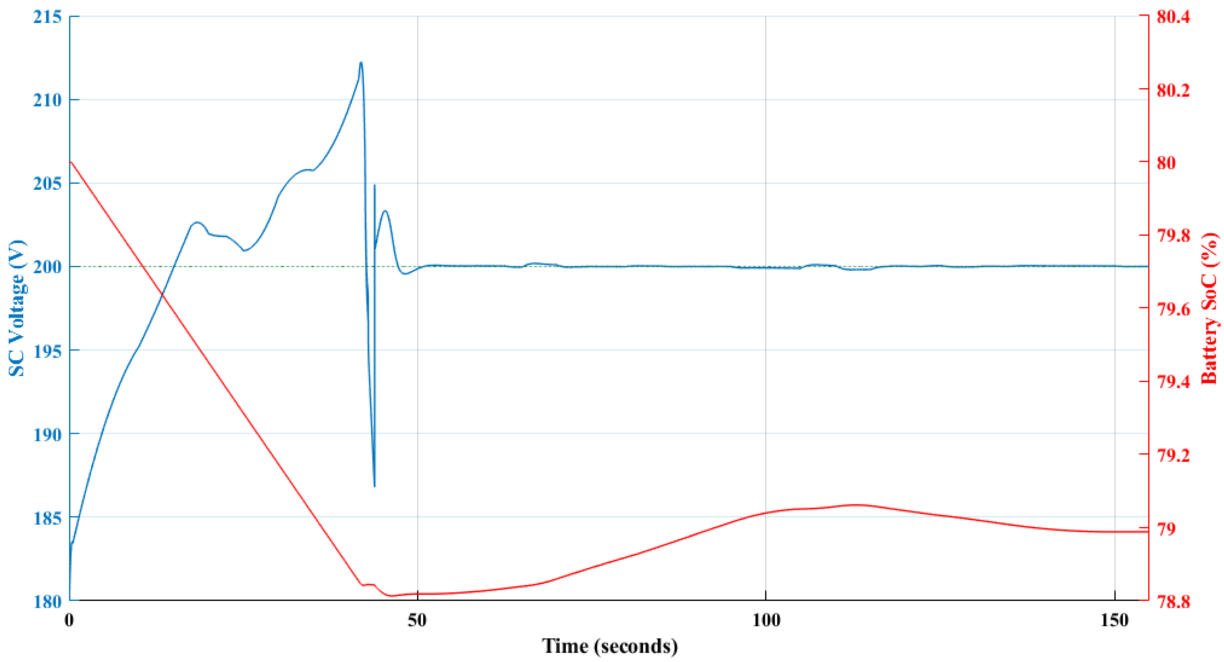

Figure 14. The SC voltage and the battery SoC using the optimized flat controller.

5. Conclusions

This research provided an effective energy management strategy for an electric vehicle powered by a hybrid power system (HPS). The hybrid power system comprises a lithium-ion battery and a supercapacitor (SC) bank. The main objective is to deliver high-quality power to the traction system. This suggested energy management aims to attenuate the bus voltage fluctuations while satisfying the load demand under different driving profiles. Enhancing the power quality will extend the battery lifecycle and improve driving performance. A flatness-based control theory has been used in his study. The controller parameters are extracted using the particle swarm optimization algorithm. Its performance has been investigated with different population sizes and the number of iterations. This study will look at how they affect controller performance. According to the obtained results, the number of iterations substantially impacts the algorithms' performance in determining the appropriate settings for the controller. The results show that combining flatness theory and a metaheuristic optimization algorithm can produce superior power quality. The suggested management algorithm provides efficient power sharing while protecting power sources and delivering excellent power quality. The obtained parameters are obtained based on the objective function, which is based on the usage model.

Based on the no-free-lunch theory, other metaheuristic optimization algorithms can better optimize the flat controller. This will be investigated in our following work. In addition, applying these strategies to online applications is a challenging task. The online processing of the objective function requires a fast calculation processor. Increasing the number of iterations or the population time requires more calculation time, which may affect the optimization performance. Therefore, a reasonable combination between the population size and the iteration number regarding the physical limitations of the calculator is needed.

Author Contributions: Conceptualization, H.R.; methodology, H.R. and R.M.G.; software, H.R. and R.M.G.; formal analysis, H.R. and R.M.G.; investigation, H.R. and R.M.G.; writing—original draft preparation, H.R. and R.M.G.; writing—review and editing, H.R. and R.M.G. All authors have read and agreed to the published version of the manuscript.

Funding: This study is supported via funding from Prince sattam bin Abdulaziz University project number (PSAU/2023/R/1445).

Data Availability Statement: Not applicable.

Acknowledgments: This study is supported via funding from Prince sattam bin Abdulaziz University project number (PSAU/2023/R/1445).

Conflicts of Interest: The authors declare no conflict of interest.

References

1. Canzler, W.; Engels, F.; Rogge, J.-C.; Simon, D.; Wentland, A. From "Living Lab" to Strategic Action Field: Bringing Together Energy, Mobility, and Information Technology in Germany. *Energy Res. Soc. Sci.* **2017**, *27*, 25–35. [CrossRef]
2. Muratori, M.; Jadun, P.; Bush, B.; Bielen, D.; Vimmerstedt, L.; Gonder, J.; Gearhart, C.; Arent, D. Future Integrated Mobility-Energy Systems: A Modeling Perspective. *Renew. Sustain. Energy Rev.* **2020**, *119*, 109541. [CrossRef]
3. Leal Filho, W.; Abubakar, I.R.; Kotter, R.; Grindsted, T.S.; Balogun, A.-L.; Salvia, A.L.; Aina, Y.A.; Wolf, F. Framing Electric Mobility for Urban Sustainability in a Circular Economy Context: An Overview of the Literature. *Sustainability* **2021**, *13*, 7786. [CrossRef]
4. Szumska, E.M. Electric Vehicle Charging Infrastructure along Highways in the EU. *Energies* **2023**, *16*, 895. [CrossRef]
5. Berckmans, G.; Messagie, M.; Smekens, J.; Omar, N.; Vanhaverbeke, L. Cost Projection of State of the Art Lithium-Ion Batteries for Electric Vehicles Up to 2030. *Energies* **2017**, *10*, 1314. [CrossRef]
6. Islam, E.S.; Moawad, A.; Kim, N.; Rousseau, A. Vehicle Electrification Impacts on Energy Consumption for Different Connected-Autonomous Vehicle Scenario Runs. *World Electr. Veh. J.* **2019**, *11*, 9. [CrossRef]
7. Vijayagopal, R.; Rousseau, A. Benefits of Electrified Powertrains in Medium- and Heavy-Duty Vehicles. *World Electr. Veh. J.* **2020**, *11*, 12. [CrossRef]
8. Hannan, M.A.; Hoque, M.M.; Mohamed, A.; Ayob, A. Review of Energy Storage Systems for Electric Vehicle Applications: Issues and Challenges. *Renew. Sustain. Energy Rev.* **2017**, *69*, 771–789. [CrossRef]
9. Song, Z.; Li, J.; Han, X.; Xu, L.; Lu, L.; Ouyang, M.; Hofmann, H. Multi-Objective Optimization of a Semi-Active Battery/Supercapacitor Energy Storage System for Electric Vehicles. *Appl. Energy* **2014**, *135*, 212–224. [CrossRef]
10. Yan, X.; Patterson, D. Improvement of Drive Range, Acceleration and Deceleration Performance in an Electric Vehicle Propulsion System. In Proceedings of the 30th Annual IEEE Power Electronics Specialists Conference. Record. (Cat. No.99CH36321), Charleston, SC, USA, 1 July 1999; IEEE: Piscataway, NJ, USA, 1999; Volume 2, pp. 638–643.
11. Kuperman, A.; Aharon, I. Battery–Ultracapacitor Hybrids for Pulsed Current Loads: A Review. *Renew. Sustain. Energy Rev.* **2011**, *15*, 981–992. [CrossRef]
12. Song, Z.; Hofmann, H.; Li, J.; Hou, J.; Zhang, X.; Ouyang, M. The Optimization of a Hybrid Energy Storage System at Subzero Temperatures: Energy Management Strategy Design and Battery Heating Requirement Analysis. *Appl. Energy* **2015**, *159*, 576–588. [CrossRef]
13. Song, Z.; Li, J.; Hou, J.; Hofmann, H.; Ouyang, M.; Du, J. The Battery-Supercapacitor Hybrid Energy Storage System in Electric Vehicle Applications: A Case Study. *Energy* **2018**, *154*, 433–441. [CrossRef]
14. Thounthong, P.; Sikkabut, S.; Mungporn, P.; Nahid-Mobarakeh, B.; Pierfederici, S.; Davat, B. Nonlinear Control Algorithm of Supercapacitor/Li-Ion Battery Energy Storage Devices for Fuel Cell Vehicle Applications. In Proceedings of the 2014 10th France-Japan/8th Europe-Asia Congress on Mecatronics (MECATRONICS2014-Tokyo), Tokyo, Japan, 27–29 November 2014; IEEE: Piscataway, NJ, USA; pp. 232–237.
15. Ferahtia, S.; Djerioui, A.; Zeghlache, S.; Houari, A. A Hybrid Power System Based on Fuel Cell, Photovoltaic Source and Supercapacitor. *SN Appl. Sci.* **2020**, *2*, 940. [CrossRef]
16. Zhang, X.; Mi, C. *Vehicle Power Management*; Power Systems; Springer: London, UK, 2011; ISBN 978-0-85729-735-8.
17. Tabbache, B.; Djebarri, S.; Kheloui, A.; Benbouzid, M. A Power Presizing Methodology for Electric Vehicle Traction Motors. *Int. Rev. Model. Simul.* **2013**, *6*, 195–202.
18. Fotouhi, A.; Auger, D.J.; Propp, K.; Longo, S.; Wild, M. A Review on Electric Vehicle Battery Modelling: From Lithium-Ion toward Lithium-Sulphur. *Renew. Sustain. Energy Rev.* **2016**, *56*, 1008–1021. [CrossRef]
19. Shepherd, C.M. Design of Primary and Secondary Cells: II. An Equation Describing Battery Discharge. *J. Electrochem. Soc.* **1965**, *112*, 657–664. [CrossRef]
20. Raza, W.; Ali, F.; Raza, N.; Luo, Y.; Kim, K.-H.; Yang, J.; Kumar, S.; Mehmood, A.; Kwon, E.E. Recent Advancements in Supercapacitor Technology. *Nano Energy* **2018**, *52*, 441–473. [CrossRef]
21. Cabrane, Z.; Lee, S.H. Electrical and Mathematical Modeling of Supercapacitors: Comparison. *Energies* **2022**, *15*, 693. [CrossRef]

22. Zandi, M.; Payman, A.; Martin, J.-P.; Pierfederici, S.; Davat, B.; Meibody-Tabar, F. Energy Management of a Fuel Cell/Supercapacitor/Battery Power Source for Electric Vehicular Applications. *IEEE Trans. Veh. Technol.* **2011**, *60*, 433–443. [CrossRef]
23. Thounthong, P.; Sikkabut, S.; Mungporn, P.; Piegari, L.; Nahid-Mobarakeh, B.; Pierfederici, S.; Davat, B. DC Bus Stabilization of Li-Ion Battery Based Energy Storage for a Hydrogen/Solar Power Plant for Autonomous Network Applications. *IEEE Trans. Ind. Appl.* **2015**, *51*, 2717–2725. [CrossRef]
24. Thounthong, P.; Tricoli, P.; Davat, B. Performance Investigation of Linear and Nonlinear Controls for a Fuel Cell/Supercapacitor Hybrid Power Plant. *Int. J. Electr. Power Energy Syst.* **2014**, *54*, 454–464. [CrossRef]
25. Kennedy, J.; Eberhart, R. Particle Swarm Optimization. In Proceedings of the ICNN'95—International Conference on Neural Networks, Perth, WA, Australia, 27 November–1 December 1995; IEEE: Piscataway, NJ, USA, 1995; Volume 4, pp. 1942–1948.
26. Yaqoob, S.J.; Ferahtia, S.; Obed, A.A.; Rezk, H.; Alwan, N.T.; Zawbaa, H.M.; Kamel, S. Efficient Flatness Based Energy Management Strategy for Hybrid Supercapacitor/Lithium-Ion Battery Power System. *IEEE Access* **2022**, *10*, 132153–132163. [CrossRef]
27. Wolpert, D.H.; Macready, W.G. No Free Lunch Theorems for Optimization. *IEEE Trans. Evol. Comput.* **1997**, *1*, 67–82. [CrossRef]
28. Janulin, M.; Vrublevskyi, O.; Prokhorenko, A. Energy Minimization in City Electric Vehicle Using Optimized Multi-Speed Transmission. *Int. J. Automot. Mech. Eng.* **2022**, *19*, 9721–9733. [CrossRef]